JOURNAL OF RHEOLOGY

The matching of polymer solution fast filament stretching, relaxation, and break up experimental results with 1D and 2D numerical viscoelastic simulation

D. C. Vadillo, M. Tembely, N. F. Morrison, O. G. Harlen, M. R. Mackley et al.

Citation: J. Rheol. **56**, 1491 (2012); doi: 10.1122/1.4749828
View online: http://dx.doi.org/10.1122/1.4749828
View Table of Contents: http://www.journalofrheology.org/resource/1/JORHD2/v56/i6
Published by the The Society of Rheology

Related Articles

Superensembles of linear viscoelastic models of polymer melts
J. Rheol. 56, 279 (2012)

Evaluation of molecular linear viscoelastic models for polydisperse H polybutadienes
J. Rheol. 55, 1341 (2011)

Solution and melt viscoelastic properties of controlled microstructure poly(lactide)
J. Rheol. 55, 987 (2011)

Influence of annealing on linear viscoelasticity of carbon black filled polystyrene and low-density polyethylene
J. Rheol. 55, 965 (2011)

The rheological characterization of linear viscoelasticity for ink jet fluids using piezo axial vibrator and torsion resonator rheometers
J. Rheol. 54, 781 (2010)

Additional information on J. Rheol.

Journal Homepage: http://www.journalofrheology.org/
Journal Information: http://www.journalofrheology.org/about
Top downloads: http://www.journalofrheology.org/most_downloaded
Information for Authors: http://www.journalofrheology.org/author_information

ADVERTISEMENT

Downloaded 22 Dec 2012 to 109.154.120.51. Redistribution subject to SOR license or copyright; see http://www.journalofrheology.org/masthead

The matching of polymer solution fast filament stretching, relaxation, and break up experimental results with 1D and 2D numerical viscoelastic simulation

D. C. Vadillo[a)]

Department of Chemical Engineering and Biotechnology, University of Cambridge, Cambridge CB2 3RA, United Kingdom

M. Tembely[b)]

Laboratory for Geophysical and Industrial Flow (LEGI, UMR 5519), University Joseph Fourier, Grenoble, BP 53, 38041 Grenoble Cedex, France

N. F. Morrison and O. G. Harlen

School of Mathematics, University of Leeds, Leeds LS2 9JT, United Kingdom

M. R. Mackley

Department of Chemical Engineering and Biotechnology, University of Cambridge, Cambridge CB2 3RA, United Kingdom

A. Soucemarianadin[c)]

Laboratory for Geophysical and Industrial Flow (LEGI, UMR 5519), University Joseph Fourier, Grenoble, BP 53, 38041 Grenoble Cedex, France

(Received 5 February 2012; final revision received 6 August 2012; published 18 September 2012)

Synopsis

This paper is concerned with the comparison of two numerical viscoelastic strategies for predicting the fast filament stretching, relaxation, and break up of low viscosity, weakly elastic polymeric fluids. Experimental data on stretch, relaxation, and breakup were obtained using a Cambridge Trimaster for a Newtonian solvent (diethyl phthalate) and three monodisperse polystyrene polymer solutions. Two numerical codes were tested to simulate the flow numerically. One code used a one-dimensional approximation coupled with the arbitrary Lagrangian–Eulerian approach and the

[a)]Author to whom correspondence should be addressed; present address: AkzoNobel Research, Development and Innovation, Stoneygate Lane, Felling, Gateshead NE10 0JY, United Kingdom; electronic mail: damien.vadillo@googlemail.com

[b)]Present address: Department of Mechanical and Industrial Engineering, Concordia University, Montreal, Quebec H3G 1M8, Canada.

[c)]Presently in delegation at Campus France, Paris, France.

© 2012 by The Society of Rheology, Inc.

Downloaded 22 Dec 2012 to 109.154.120.51. Redistribution subject to SOR license or copyright; see http://www.journalofrheology.org/masthead

other a two-dimensional axisymmetric approximation for the flow. In both cases, the same constitutive equations and mono and multimode parameter fitting were used, thereby enabling a direct comparison on both codes and their respective fit to the experimental data. Both simulations fitted the experimental data well and surprisingly the one-dimensional code closely matched that of the two-dimensional. In both cases, it was found necessary to utilize a multimode approach to obtain a realistic match to the experimental data. The sensitivity of the simulation to the choice of constitutive equation (Oldroyd-B and FENE-CR) and the magnitude of nonlinear parameters were also investigated. The results are of particular relevance to ink-jet processing and demonstrate that high shear rate, low viscosity viscoelastic polymeric flows can be simulated with reasonable accuracy. © *2012 The Society of Rheology*. [http://dx.doi.org/10.1122/1.4749828]

I. INTRODUCTION

The way in which viscoelastic fluids stretch, thin, and break up is of relevance to a number of technologies and these three phases of the flow have in the past received extensive scientific attention although generally as three different individual topics. The stretching of polymeric fluids in particular has received detailed experimental and modeling attention in the last decade from among others [Anna and McKinley (2001); McKinley and Sridhar (2002); Bach *et al*. (2002); Clasen *et al*. (2006a); Clasen *et al*. (2006b)] where the work has concentrated on determining the transient extensional viscosity of fluids. The thinning of prestretched polymeric fluids has also been investigated experimentally following pioneering experimental work by Bazilevsky *et al*. (1997), which was subsequently modeled by Entov and Hinch (1997). A review by McKinley (2005b) gives an authoritative account of factors that influence filament thinning behavior. Filament breakup is a delicate process and is the least well characterized and modeled of the three topics among stretching, relaxation, and breakup covered by this paper.

Ink-jet printing can involve all three elements mentioned above during filament formation and droplet breakup [Dong *et al*. (2006); Hoath *et al*. (2009); Jang *et al*. (2009)]. Although filament thinning experiment cannot reach filament stretching strain rate anywhere near inkjet printing processing, it enables measuring very short extensional relaxation time with timescale comparable with inkjet droplet formation [Vadillo *et al*. (2012)]. It also gives access to the elasto-capillary times controlling filament behavior and breakup process [Tembely *et al*. (2011)]. As such, filament thinning simulations are therefore a way to test different constitutive equations with well controlled boundary conditions which may eventually lead to a better understanding of the inkjet process which is much more challenging by itself. In order to mimic elements of this complex deformation process, a "Cambridge Trimaster (CTM)" geometry apparatus was developed specifically as a device to capture aspects of the process with well-defined boundary conditions [Vadillo *et al*. (2010b)]. The CTM has strong similarity to the single piston Rozhkov filament thinning device [Bazilevsky *et al*. (1990)] and the Haake Caber filament thinning apparatus (http://www.thermo.com/com/cda/product/detail/). The twin piston Trimaster was developed specifically for low viscosity fluids with a fast, controlled initial displacement and for use with high speed photography [Vadillo *et al*. (2010b)].

Characterization of low viscosity, linear viscoelasticity with short relaxation times is a challenging area of rheology; however, the Pechold, piezo axial vibrator (PAV) [Groß *et al*. (2002); Kirschenmann (2003); Crassous *et al*. (2005); Vadillo *et al*. (2010a)] is an apparatus that can probe fluid within the range of millisecond relaxation times. Thus by using a combination of the CTM and the PAV, it was possible to probe both the extensional filament break up behaviors of viscoelastic fluids that are well characterized, at least in the linear viscoelastic (LVE) regime using the PAV.

Downloaded 22 Dec 2012 to 109.154.120.51. Redistribution subject to SOR license or copyright; see http://www.journalofrheology.org/masthead

In a recent work, some authors of this paper have published the matching of experimental and simulation filament stretching and thinning data using the single mode Maxwell description for the viscoelastic contribution of the fluid [Tembely *et al.* (2012)]. The results were promising, although all the elements of the Trimaster data with a single mode one-dimensional (1D) simulation of the process of thinning and break up could not be fully captured. A direct comparison between 1D and two-dimensional (2D) models may be found in the work of Yildirim and Basaran (2001) and more recently by Furlani and Hanchak (2011). The latter authors have used the slender jet 1D approximation and solved the arising nonlinear partial differential equations (PDE) using the method-of lines wherein the PDEs are transformed to a system of ordinary differential equations for the nodal values of the jet variables on a uniform staggered grid. The results are impressive with the key advantages being the ease of implementation and the speed of computation albeit in a different configuration than the problem considered in this paper. In the present paper, Trimaster data for polymer solutions are matched to single and multimode viscoelastic simulation data, using both a computationally time efficient 1D simulation and a potentially more rigorous 2D simulation. The paper represents a "state of art" position in matching extensional time dependent results with high level numerical simulation, thereby enabling the effects of constitutive equation and constitutive parameters to be tested.

II. TEST FLUIDS, RHEOLOGICAL CHARACTERIZATION, AND TRIMASTER EXPERIMENTAL PROTOCOLS

A. Test fluid preparation and characterization

The fluids used were a series of mono-disperse polystyrene dissolved in diethyl phthalate (DEP) solvent as previously described in Vadillo *et al.* (2010a) and Vadillo *et al.* (2010b). Near mono disperse polystyrene (PS) polymer was manufactured specially by Dow, and gel permeation chromatography (GPC) with tetrahydrofuran (THF) as the solvent enabled determination of mass and number average molecular weights M_w and M_n as 110 and 105 kg/mol, respectively. A stock solution of PS dilution series was prepared by adding 10 wt. % of PS to the DEP at ambient temperature. The resulting solution was heated to 180 °C and stirred for several hours until the polymer was fully dissolved. The dilution series were prepared by subsequent dilution of the respective stock solutions. Sample surface tension remained constant at 37 mN/m up to 10 wt. % PS110 concentration and with a critical polymer overlap concentration c* of 2.40 wt. % [Clasen *et al.* (2006a)]. The zero shear viscosities η_0 of the solutions were determined from PAV low frequency complex viscosity η^* data within the terminal relaxation regime and the measured viscosities are given in Table I.

B. Rheological characterization

The PAV has been used to characterize the LVE behavior of samples with viscosity as low as 1 mPa s on a frequency range comprised between 0.1 and 10 000 Hz [Groß *et al.* (2002); Kirschenmann (2003); Crassous *et al.* (2005); Vadillo *et al.* (2010a)]. The PAV measures the complex modulus G^* of the test fluid with $G^* = G' + iG''$ and where G' is the storage modulus and G'' is the loss modulus. The complex viscosity η^* is related to the complex modulus by $\eta^* = G^*/\omega$, where ω is the angular frequency. Experimental LVE results are presented in Fig. 1. Loss modulus G'' and elastic modulus G' have been found to increase with the frequency and to vertically shift with the polymer addition. Note that the pure DEP solvent does not show any G′. Both moduli approach at lower

Downloaded 22 Dec 2012 to 109.154.120.51. Redistribution subject to SOR license or copyright; see http://www.journalofrheology.org/masthead

TABLE I. Zero shear rate complex viscosity of the different polymer solutions at 25 °C.

Solvent	M_w (g/mol)	C (wt. %)	η^* (mPa s)
DEP	110 000	0	10
DEP	110 000	1	15.2
DEP	110 000	2.5	31.5
DEP	110 000	5	69

frequencies the terminal relaxation regime with the expected scaling with a power of 1 for the loss modulus [Fig. 1(a)], and a power of 2 for the storage modulus [Fig. 1(b)], and a constant complex viscosity η^* in this regime as shown in Fig. 1(c) (except for 5 wt. % PS110 after 2000 Hz). The experimental results are displayed between 10^2 and 10^4 Hz, the range on which the storage modulus has been captured. At lower frequency, the fluids have been found essentially to behave as a Newtonian fluid with the presence of a loss modulus only.

C. CTM experimental protocol

The CTM is a capillary breakup extensional rheometer that has been specifically designed to probe the extensional rheology of weakly viscoelastic fluids. This apparatus performs a fast stretch of a cylinder of fluid initially located between two identical pistons over a short distance. This apparatus and its limitation have been presented in details in Vadillo *et al.* (2010b) In the present study, the piston diameters are 1.2 mm and the experimental filament stretching conditions are an initial gap size L_0 of 0.6 mm and a stretching distance L_f of 0.8 mm at a relative piston speed $2V_p$ of 150 mm/s. This corresponds to a filament strain rate $2V_p/L_0 = 250\,s^{-1}$ and a filament aspect ratio L_f/L_0 of 2.3. The piston velocity and stretching distance have been chosen to ensure that pistons stop their motions before the critical time scale for inertio-capillary break up for the sample with the lower viscosity, here the DEP. For such a fluid, this time scale has been estimated around 5 ms [Tembely *et al.* (2012)]. These conditions will be conserved in the following for both experiments and simulations.

The transient filament profiles have been captured using a Photron Fastcam (http://www.photron.com/index.php?cmd=product_general&product_id=1) 1024 PCI high speed camera at 6000 fps, for a picture size of 128 × 256 with a shutter time of 3 μs. The filament thinning measurement, as well as the filament breakup behavior, was obtained using automatic image processing based on grayscale variation throughout image for edge detection and the minimum diameter that can be resolved was about 6 μm.

D. Relaxation time and moduli determination

Relaxation spectrum determination from LVE measurements is an ill-posed problem and has been studied extensively in the literature [see, for example, Baumgaertel and Winter (1989); Kamath *et al.* (1990); Stadler and Bailly (2009)] and different techniques from linear to nonlinear regression have been developed to obtain relaxation spectra from oscillatory LVE data. In the modeling carried out here, a series of equidistant relaxation times spaced on the logarithmic scale were chosen with one mode per decade. This was motivated by the fact that, in experiments, low viscoelastic fluids have shown significant differences between relaxation times in shear and in extension [Clasen *et al.* (2006a)], and recent simulations have shown that using a single mode Maxwell description of the fluid was not sufficient [Tembely *et al.* (2012)] to capture those differences. The

Downloaded 22 Dec 2012 to 109.154.120.51. Redistribution subject to SOR license or copyright; see http://www.journalofrheology.org/masthead

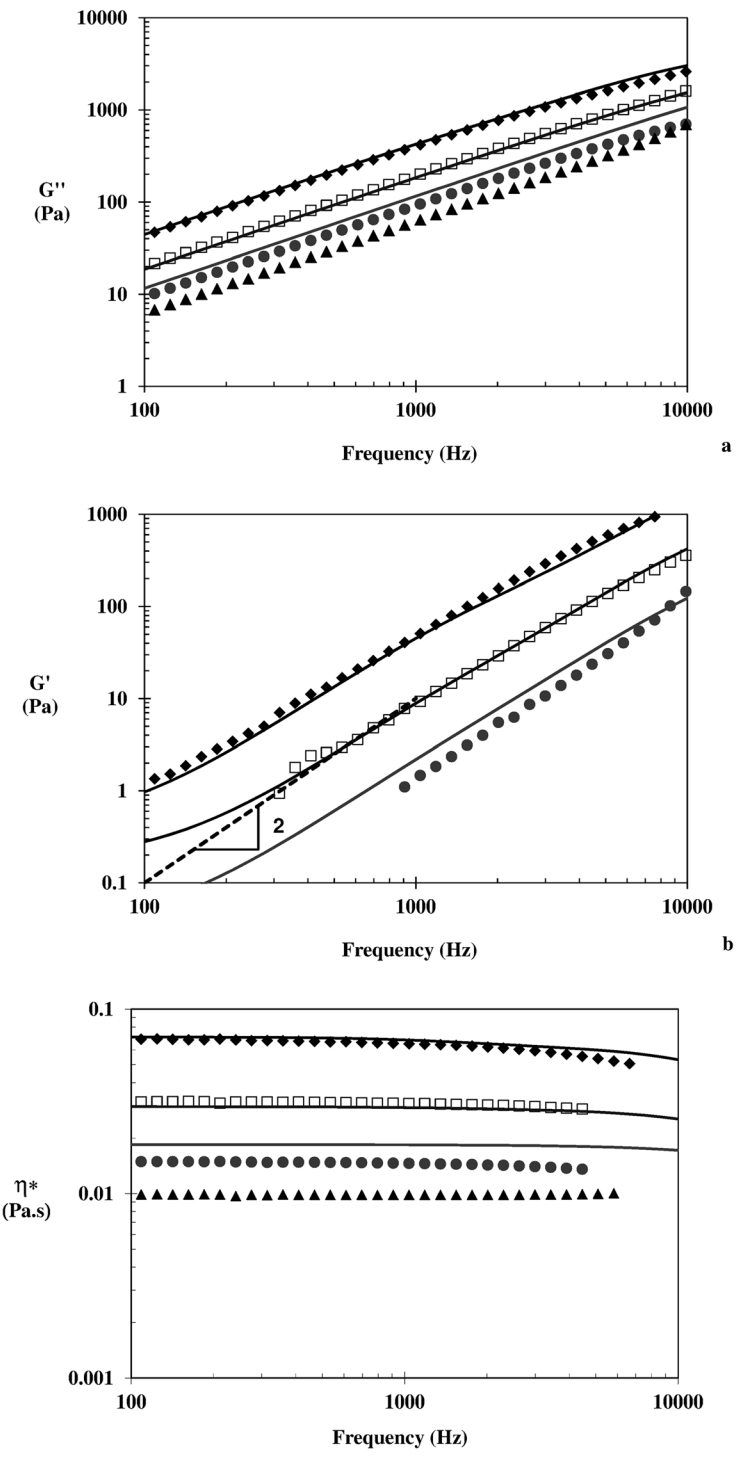

FIG. 1. Evolution of (a) loss modulus G″, (b) elastic modulus G′, and (c) complex viscosity η^* as a function frequency for DEP-PS 110 000 solutions at different concentrations. (▲) DEP, (●) DEP-1 wt. % PS110, (□) DEP-2.5 wt. % PS110, and (◆) DEP-5 wt. % PS110. Solid line represents the multimode optimization results while the dashed line on G′ graph corresponds to a power law function of index 2.

Downloaded 22 Dec 2012 to 109.154.120.51. Redistribution subject to SOR license or copyright; see http://www.journalofrheology.org/masthead

minimization program for both G' and G'' data was solved using MATLAB®. The solution involved the use of SQP (sequential quadratic programming) [Jorge and Wright (2006)] methods, which may be considered as a state of the art nonlinear programming optimization technique. This method has been shown to outperform other methods in terms of accuracy, efficiency, and adaptability over a large number of problems [Schittkowski (1985)] and it is an effective method for nonlinear optimization with constraints. In each iteration, the nonlinear problem was approximated using a quadratic which is easy to solve (hence the name SQP).

The conversion of the experimental data (G'_{m}, G''_{m}, ω_j) into a relaxation function was performed by expressing $G(t)$ as a discrete relaxation spectrum (g_i, λ_i). The Maxwell model relates the real and imaginary parts of the complex modulus determined in LVE measurement to the discrete relaxation spectrum of N relaxation times λ_i and a relaxation strengths g_i through

$$G'(\omega) = \sum_{i=1}^{N} g_i \frac{(\omega\lambda_i)^2}{1+(\omega\lambda_i)^2}, \tag{1}$$

$$G''(\omega) = \eta_s\omega + \sum_{i=1}^{N} g_i \frac{\omega\lambda_i}{1+(\omega\lambda_i)^2} \tag{2}$$

with ω being the angular frequency of the experiment, and N is the number of relaxation modes. As indicated in (2), G'' accounts for the solvent viscosity.

Generally, the spectra can be computed by minimizing the "least mean square error" as follows [Bird *et al*. (1987); Stadler and Bailly (2009)]:

$$D = \sum_{j=1}^{M} \left[\frac{G'(\omega_j)}{G'_m(\omega_j)} - 1\right]^2 + \left[\frac{G''(\omega_j)}{G''_m(\omega_j)} - 1\right]^2, \tag{3}$$

where M is the number of measurements.

The model is initialized by choosing the relaxation times to be equidistantly spaced on a logarithmic scale such that $\log(\lambda_i/\lambda_{i+1}) = 1/p$. Setting $p=1$, i.e, one mode per decade, has been found to provide sufficient accuracy to accurately describe the LVE behavior (Fig. 1). In the numerical simulation, the Maxwell component of the model was fitted with five modes. The relaxation times are chosen such that G' and G'' measured over the frequency range $\omega_{\min} < \omega < \omega_{\max}$ recover all the information regarding the relaxation spectrum over the range $1/\omega_{\max} < \lambda_i < 1/\omega_{\min}$; however, the correct range is given by $e^{\pi/2}/\omega_{\max} < \lambda_i < e^{-\pi/2}/\omega_{\min}$ [Davies and Anderssen (1997)]. This spectrum is a generalized form of the Maxwellian dynamics [Ferry (1980)] and shown in Table II.

III. GENERAL EQUATIONS AND NUMERICAL SIMULATIONS

Numerical simulations of the Trimaster deformation were performed using both a 1D model and a 2D axisymmetric model. In Subsections III A–III D, the general equations and the numerical techniques used in both cases are detailed.

A. Flow geometry

To model the experimental conditions, an initial cylindrical column of fluid was considered bounded by two rigid circular pistons of diameter D_0. The fluid and the pistons were initially at rest; subsequently, the pistons moved vertically outwards with time-

Downloaded 22 Dec 2012 to 109.154.120.51. Redistribution subject to SOR license or copyright; see http://www.journalofrheology.org/masthead

TABLE II. Relaxation time and shear modulus obtained from Maxwell model fit of the PAV data for the different samples.

λ_i (μs)	1% PS g_i (Pa)	2.5% PS g_i (Pa)	5% PS g_i (Pa)	10% PS g_i (Pa)
1	7.789	83.8229	397.9015	1086.4419
10	428.76	1450.8952	4680.9517	9126.8723
100	1.6435	10.5177	93.1172	2012.6511
1000	0	0	0	16.4133
10 000	0.0342	0.1855	0.4288	0.4291

dependent velocities $V_p(t)$ (top piston) and $-V_p(t)$ (bottom piston), which are prescribed functions based on fitting a smooth tanh curves through measurements of the Trimaster piston motion in the experiments. As described in Tembely *et al.* (2011), the form of tanh has been chosen to fit the symmetrical "S" shape experimentally observed for the piston motion with time. In they work, the authors have shown that the use of an accurate representation of the piston dynamic response is of importance in the simulation of fast transient dynamic of low viscosity and/or low viscoelasticity fluids.

Using a cylindrical coordinate system $\{r, \theta, z\}$, the flow was constrained to be axisymmetric so that all flow fields are independent of the angular coordinate θ, and the simulation may be restricted to the rz-plane. The coordinate origin is at the axis of the jet, midway between the initial positions of the two pistons. Figure 2 shows a schematic diagram of the computational domain at an intermediate stage of the piston motion.

Symmetric boundary conditions are required along the z-axis to maintain axisymmetry, and conditions of no-slip were applied at each piston surface. The boundary conditions at the free surface are those of zero shear stress and the interfacial pressure discontinuity due to the surface curvature

$$\mathbf{t}.\underline{\underline{\mathbf{T}}}.\mathbf{n} = 0 \quad \text{and} \quad [\underline{\underline{\mathbf{T}}}.\mathbf{n}]_{\text{air}}^{\text{fluid}} = -\gamma\kappa, \tag{4}$$

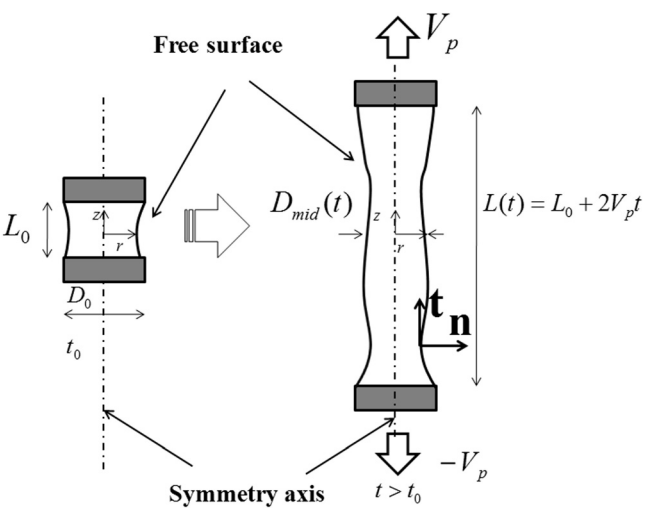

FIG. 2. Diagram of filament stretch and thinning geometry and the computational domain, shown midway through the stretching phase as the pistons move outwards and the fluid column necks in the middle. Initially, the fluid column is cylindrical. Extracted from [Tembely *et al.* (2012)].

Downloaded 22 Dec 2012 to 109.154.120.51. Redistribution subject to SOR license or copyright; see http://www.journalofrheology.org/masthead

where $\underline{\underline{\mathbf{T}}}$ is the total stress tensor, $\mathbf{n}$ is the unit vector normal to the free surface (directed outward from the fluid), $\mathbf{t}$ is the unit tangent vector to the free surface in the rz-plane, γ is the coefficient of surface tension, and κ is the curvature of the interface. It is assumed that the external air pressure is a negligible constant.

The location of the free surface at each time-step was determined implicitly via a kinematic condition. In the axisymmetric simulations, this was realized automatically, since the mesh is Lagrangian and the mesh nodes are advected with the local fluid velocity. The contact lines between the free surface and the pistons were held pinned at the piston edges throughout.

The initial conditions are that the fluid is at rest ($\mathbf{v} = \mathbf{0}$) and the polymer is at unstretched equilibrium ($\mathbf{A}_i = \mathbf{I}$).

B. Governing equations

The governing equations for incompressible isothermal flow of a viscoelastic fluid are the classical Navier–Stokes equations for Newtonian fluids together with an additional viscoelastic term coming from the extra stress tensor $\underline{\underline{\boldsymbol{\sigma}}}$. The momentum conservation then may be expressed as follows in which the third term on right-hand side accounts for viscoelasticity:

$$\rho \frac{d\mathbf{v}}{dt} + \rho(\mathbf{v}.\nabla)\mathbf{v} = -\nabla p + \eta_s \nabla^2 \mathbf{v} + \nabla.\underline{\underline{\boldsymbol{\sigma}}} + \rho g \mathbf{z} \tag{5}$$

and the continuity equation reads

$$\nabla.\mathbf{v} = 0, \tag{6}$$

where p is the fluid pressure, ρ is the fluid density, η_s is the solvent viscosity, and g is the acceleration due to gravity.

C. Constitutive equations

For the viscoelastic fluid models, the polymer contribution was described by a finitely extensible nonlinear elastic (FENE) dumbbell model which makes use of the conformation tensor $\mathbf{A}$, and the stress tensor reads [see, for example, Chilcott and Rallison (1988)]

$$\boldsymbol{\sigma} = Gf(R)(\mathbf{A} - \mathbf{I}), \tag{7}$$

where G is the elastic modulus, $f(R)$ is the finite extensibility factor related to the finite extensibility parameter L, representing the ratio of a fully extended polymer (dumbbell) to its equilibrium length, and $R = \mathrm{Tr}(A)$. L can be described in terms of molecular parameters as

$$L = \sqrt{3}\left[\frac{j\left(\sin\frac{\theta}{2}\right)^2 M_w}{C_\infty M_u}\right]^{1-\nu}. \tag{8}$$

In this expression, θ corresponds to the C–C bond angle and is equal to 109.5°, j corresponds to the number of bonds (2 in the case of PS) of a monomer of molar mass $M_\mathrm{u} = 104$ g/mol, C_∞ is the characteristic ratio for a given polymer equal to 9.6, M_w is the molecular weight of the polymer, and ν is the excluded volume exponent equals to 0.57 for PS110 [Clasen *et al.* (2006a)]. In the case where the dumbbells are infinitely

Downloaded 22 Dec 2012 to 109.154.120.51. Redistribution subject to SOR license or copyright; see http://www.journalofrheology.org/masthead

extensible, $f(R) = 1$ and the constitutive equation is that of an Oldroyd-B fluid. For PS110, L has been estimated at 15.

For a multimode model, the extra stress may be expressed as a sum of contributions from each mode. For the generalized multimode problem with N modes, each mode (i) with partial viscosity (η_i) and relaxation time (λ_i), the extra-stress tensor of the FENE-CR expresses

$$\underline{\underline{\boldsymbol{\sigma}}} = \sum_{i=1}^{N} g_i f_i(R_i)(\mathbf{A}_i - \mathbf{I}) \,, \tag{9}$$

where $f_i(R_i) = 1/(1 - R_i/L_i^2)$ with $R_i = \mathrm{Tr}(\mathbf{A}_i)$. For simplicity, it is assumed that the extensibility $L_i = L$ is constant, but other approaches may be used [Lielens *et al.* (1998)]. The dimensionless evolution equation for the ith mode is

$$\frac{d\mathbf{A}_i}{dt} = -\frac{f_i(R_i)}{\mathrm{De}_i}(\mathbf{A}_i - \mathbf{I}) \,, \tag{10}$$

where $\overset{\nabla}{\mathbf{A}}_i = \frac{d\mathbf{A}_i}{dt} - \nabla\mathbf{v}^T{}_i.\mathbf{A}_i - \mathbf{A}_i.\nabla\mathbf{v}_i$ is the Oldroyd upper-convected time derivative of A_i, and De_i is the Deborah number for the ith mode defined as follows:

$$\mathrm{De}_i = \lambda_i/\tau, \tag{11}$$

g_i and λ_i are, respectively, the moduli and relaxation times described by the multimode optimization, see Subsection II D, and where τ is the characteristic inertio-capillary time scale of the system defined by $\tau = \sqrt{\rho {R_0}^3/\gamma}$.

Scaling was performed using the piston radius R_0 as a length scale, and a characteristic speed U as a velocity scale, where U is the average piston speed in the 2D case, and $U = R_0/\tau$ in the 1D case. The time was scaled by R_0/U and τ, in the 2D and 1D cases, respectively; whereas pressures and stresses were scaled by ρU^2. The scalings yielded the dimensionless governing equations:

$$\frac{d\mathbf{v}}{dt} + (\mathrm{v}.\nabla)\mathbf{v} = -\nabla p + \frac{1}{\mathrm{Re}}\left(\nabla^2\mathbf{v} - \sum_{i=1}^{N} c_i \nabla \overset{\nabla}{\mathbf{A}}_i\right) + \frac{1}{\mathrm{Fr}^2}\mathbf{z} \,, \quad \nabla\cdot\mathbf{v} = 0 \,, \tag{12}$$

where t, $\mathbf{v}$, and p are now the dimensionless time, velocity, and pressure, respectively. For each viscoelastic mode, an additional parameter $c_i = g_i\lambda_i/\eta_\mathrm{s}$ has been introduced: It may be interpreted as a measure of the concentration (volume fraction) of dumbbell molecules corresponding to the ith mode. With the particular scalings used here, the flow is characterized by the dimensionless groups Re, We, and Fr, which are, respectively, the Reynolds, Weber, and Froude numbers:

$$\mathrm{Re} = \frac{\rho U R_0}{\eta_\mathrm{S}} \,, \quad \mathrm{We} = \frac{\rho U^2 R_0}{\gamma} \,, \quad \mathrm{Fr} = \left(\frac{U^2}{gR_0}\right)^{1/2} \,, \tag{13}$$

in addition to the Deborah number De_i for each mode, defined earlier. The Reynolds number represents the competition between the inertia and the viscosity, the Weber number the competition between the inertia and the surface tension while the Froude number represents the competition between the inertia and the gravity effects.

Another important dimensionless number is that of Ohnesorge, $Oh = \eta_\mathrm{S}/\sqrt{\rho\gamma R_0}$. With the scalings used here, the Ohnesorge number can be expressed in terms of the

Downloaded 22 Dec 2012 to 109.154.120.51. Redistribution subject to SOR license or copyright; see http://www.journalofrheology.org/masthead

Weber and Reynolds numbers: $Oh = \sqrt{We}/Re$. Alternative choices of scaling may result in other different dimensionless groupings [Eggers and Villermaux (2008)] as for example, the Capillary number (ratio between viscous forces and surface tension) and the Bond number (ratio between gravitational forces and surface tension). The Bond number and the Capillary number have been estimated at ~ 0.11 and between 0.04 and 0.28, respectively, indicating that surface tension is the dominating force and the gravitational effects negligible. An extensive discussion of dimensionless number of the problem can be found in McKinley (2005a).

D. Computational methods

1. 1D simulation

The previous equations (4)–(6) can be further simplified to retrieve the lubrication equation. The 1D simulation method follows the same approach than in the recently presented published work by Tembely *et al.* (2012) namely considering the radial expansions and taking the lower order results in r lead to the nonlinear 1D equations describing the filament dynamics [Eggers and Dupont (1994); Shi *et al.* (1994)]. The result is a system of equations for the local radius $h(z, t)$ of the fluid neck, and the average velocity $v(z, t)$ in the axial direction:

$$\partial_t h + vh' + v'\frac{h}{2} = 0, \tag{14}$$

where prime $(')$ denotes the derivative with respect to z coordinates and

$$\partial_t v + vv' = -\kappa' + 3\tilde{\nu}_s \frac{(v'h^2)'}{h^2} + \frac{1}{h^2}[h^2(\sigma_{p,zz} - \sigma_{p,rr})]'. \tag{15}$$

For the multimode 1D model in dimensionless form, the axial and radial stresses may be expressed as

$$\sigma_{p,zz} = \sum_{i=1}^{N} g_i f(R_i) A_{zz,i}, \tag{16}$$

$$\sigma_{p,rr} = \sum_{i=1}^{N} g_i f(R_i) A_{rr,i}. \tag{17}$$

As previously, the full expression of the curvature given in Eq. (18) was used to avoid instability in the solution and to provide the capability to represent a rounded drop:

$$\kappa = \frac{1}{h(1+h'2)^{1/2}} - \frac{h''}{(1+h'2)^{3/2}}. \tag{18}$$

To close the 1D model, the following boundary conditions are imposed, the no-slip conditions at the piston surfaces,

$$h(z = -L/2,t) = h(z = L/2,t) = R_0, \tag{19}$$

$$v(z = -L/2,t) = -V_p,\ v(z = L/2,t) = V_p \tag{20}$$

and a kinematic condition for the radius $h(z,t)$ of the jet may be expressed as

Downloaded 22 Dec 2012 to 109.154.120.51. Redistribution subject to SOR license or copyright; see http://www.journalofrheology.org/masthead

$$\frac{dh}{dt} = \frac{\partial h}{\partial t} + v_z \frac{\partial h}{\partial z} = v_r(r = h,t). \tag{21}$$

The governing equations in 1D simulation were solved with COMSOL (http://www.uk.comsol.com/) using the arbitrary Lagrangian–Eulerian (ALE) technique. The ALE technique is such that the computational mesh can move arbitrarily to optimize the shape of the elements, while the mesh on the boundaries follows the pistons motion. This ALE capacity implemented in the COMSOL code combined with the choice of very fine meshes enables to track the relevant physics as shown in Tembely *et al*. (2012). Due to the piston motion, the computational domain changes with time (see Fig. 3). With the ALE approach, the time derivative of any quantity is defined as $\frac{d}{dt} = \frac{\partial}{\partial t} + (\vec{v} - \vec{v}_m).\nabla$, where $\vec{v}_m$ is the mesh velocity imposed by the piston velocity.

It is worth mentioning that the stress boundaries are ignored in the 1D approach due to the weakly viscoelastic character of the samples and the initial filament aspect ratio being close to 1 [Yao and McKinley (1998)]. The 2D axisymmetric approach includes *per se* that effect.

Figure 4 presents the evolution of the simulated midfilament as a function of time for 1D and 2D simulations using different number of mesh elements. The 1D numerical results with between 240 and 3840 mesh elements do not show any difference. The results thus seem to be insensitive to mesh size as shown in Fig. 4. Similar observation is made for the 2D simulation results regardless of the initial number of mesh elements. The 2D simulation approach mesh is adaptive and evolves with time throughout the simulation resulting in a very large number of elements [see inset in Fig. 4(a)].

2. 2D simulation

An extended version of the split Lagrangian–Eulerian method of Harlen *et al*. (1995) was used. The nature of the extension was twofold: In the problems for which the method was originally developed there were no free surface boundaries, and the inertial terms were neglected ($Re = 0$). The method has since been adapted and extended to deal with

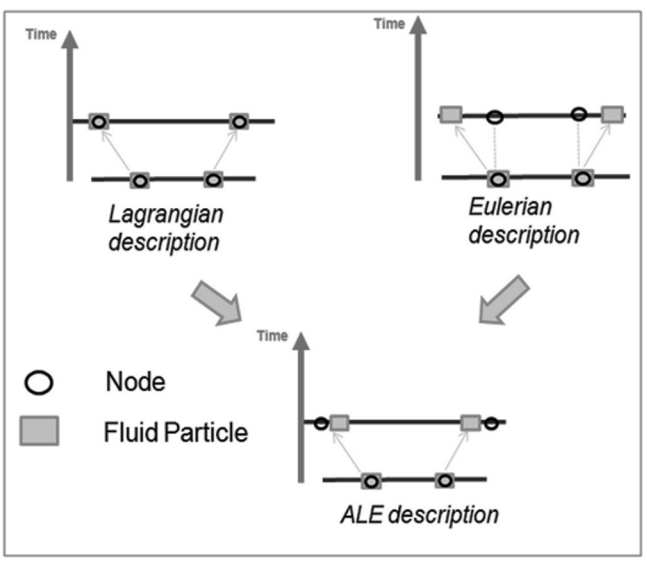

FIG. 3. Mesh evolution of the ALE method for the 1D simulation.

Downloaded 22 Dec 2012 to 109.154.120.51. Redistribution subject to SOR license or copyright; see http://www.journalofrheology.org/masthead

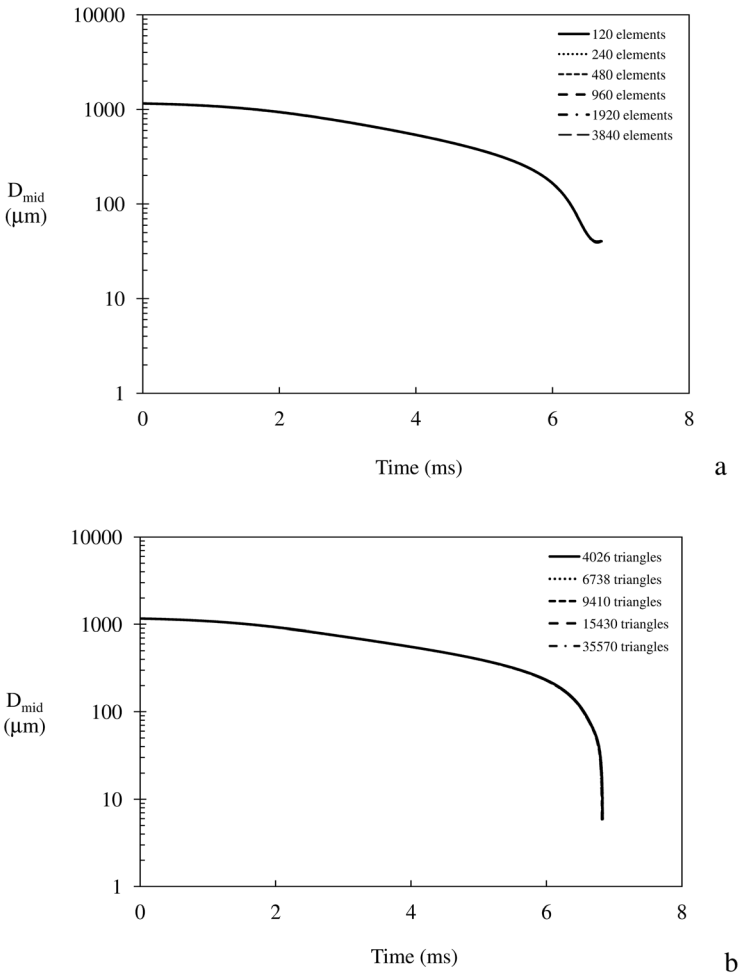

FIG. 4. Evolution of the simulated midfilament for different number of mesh elements for (a) 1D simulation approach and (b) 2D simulation approach. In the 2D simulation, the number of triangles is the one at $t = 7.2$ ms.

inertial flows and has been used to model the breakup of Newtonian and viscoelastic jets [Morrison and Harlen (2010); Castrejon-Pita *et al.* (2011)].

The velocity and pressure fields are discretized over an irregular triangular mesh of P_1–P_1 Galerkin elements; each component of the conformation tensor **A** is assigned a value for each element. An artificial stabilization was employed in order to prevent spurious numerical pressure oscillations [Brezzi and Pitkaranta (1984)]. The value of the stabilization parameter was optimized with respect to the spectral properties of the discrete coefficient matrix [Wathen and Silvester (1993)]. A theta-scheme was used for the discrete time-stepping, and the discrete governing equations were linearized via Picard iteration. For each iteration, the linear system was solved numerically using the minimal residual (MINRES) method [Paige and Saunders (1975)]. Adaptive time-stepping was controlled by a Courant-Friedrichs-Lewy [Courant *et al.* (1928)] condition. The position of each mesh node was updated after each time-step using the converged velocity solution.

The numerical integration of the evolution equation for the conformation tensor was conducted separately for each element between time-steps, by transforming to a codeforming

Downloaded 22 Dec 2012 to 109.154.120.51. Redistribution subject to SOR license or copyright; see http://www.journalofrheology.org/masthead

frame with local coordinates in each triangle. In such a frame, the upper-convected derivative $\overset{\nabla}{\mathbf{A}}$ becomes the ordinary time derivative dA/dt. Similarly, the Lagrangian derivative $D\mathbf{u}/Dt$ becomes $d\mathbf{u}/dt$. The interfacial boundary condition is handled similarly to the treatment by Westborg and Hassager (1989).

To maintain element shape quality throughout the simulations, local mesh reconnections were made between time-steps in regions where significant element distortion had occurred. The criteria for reconnection were based on the geometric optimality of the Delaunay triangulation [Edelsbrunner (2000)]. The local mesh resolution was also maintained by the addition of new nodes in depleted regions and the removal of nodes in congested regions.

In order to represent the capillary breakup of thin fluid filaments, the fluid domain was subdivided artificially when the filament radius falls below a certain threshold. This threshold has been taken as $<0.5\%$ of the piston diameter to match the smallest diameter that can be experimentally resolved ($\sim 6\ \mu$m). Below this value, the filament is not experimentally visible and is therefore considered broken. A more detailed discussion of the capability of the simulations to capture pinch-off dynamics on a finer scale is given in Castrejon-Pita *et al*. (2011).

IV. RESULTS AND DISCUSSION

A. Experimental results

Examples of the base experimental data are shown in Fig. 5 where photographs of Trimaster experiments for different polymer loading are shown as a function of time. The

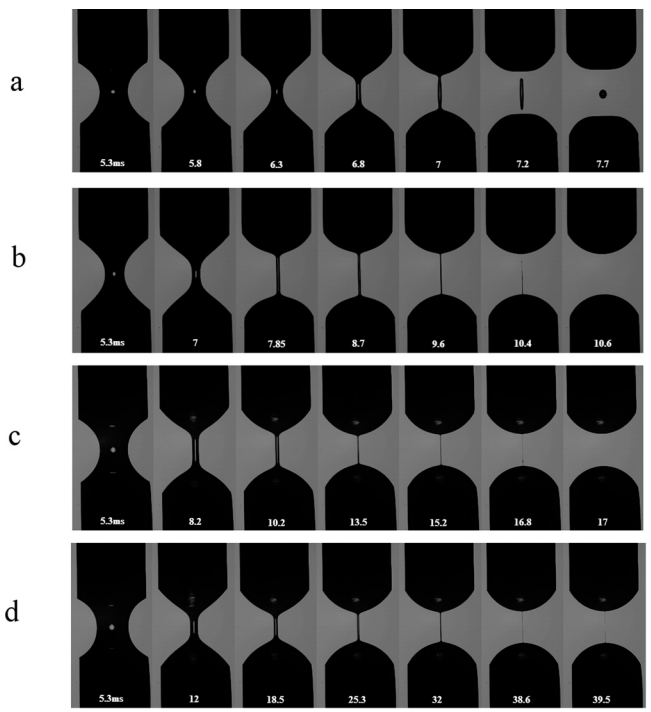

FIG. 5. Photograph of the filament stretch, thinning and break up captured with the Trimaster for (a) DEP, (b) DEP + 1 wt. % PS110, (c) DEP + 2.5. wt. % PS110, (d) DEP + 5. wt. % PS110. The first picture of each series ($t = 5.3$ ms) corresponds to the piston cessation of motion.

Downloaded 22 Dec 2012 to 109.154.120.51. Redistribution subject to SOR license or copyright; see http://www.journalofrheology.org/masthead

pure DEP solvent, shown as series 5 a, indicates a filament stretch followed by end pinching during relaxation to give a single central drop. The other extreme is shown by series 5 d for the 5% polymer loading, where stretching is followed by a progressive filament thinning with a very much longer break up time. The whole time evolution of the full profile along the thread is of general interest and importance; however, the detailed behavior of the centre line diameter will be considered beforehand.

B. Numerical results

1. Midfilament evolution

The experimental time evolution of the midpoint of the filament is given in Fig. 6 and the figure displays the characteristic feature of an increased filament life time with a progressive increase of polymer loading. It is this experimental midfilament time evolution that has been used as the basis for comparison with the 1D and 2D numerical simulations. Figure 7 shows that both the 1D and the 2D numerical simulations are in close agreement with the base case Newtonian experimental results. Both the decay profile and final 7.5 ms break point are accurately described by the simulations. Figures 7–15 present the evolution of the midfilament and not the minimum filament or the breakup point which position might vary from one case to another. The simulation breakup diameter has been set at 6 μm but might occur at the top and the bottom of the filament, as experimentally observed in the case of DEP. In such case, a droplet is formed in the middle of the filament explaining the large diameter observed experimentally and in simulations at breakup time (Figs. 5 and 7).

Single mode simulations are shown in Figs. 8–10 for 1%, 2.5%, and 5% concentration solutions, respectively. The simulations were carried out using the FENE-CR constitutive equation with the extensibility parameter $L = 30$. The extensibility value of $L = 30$ adopted in this paper has been found to provide a better match with the experimental results than the theoretic value of 15. The possible existence of higher molecular mass chains, albeit in small quantities, may justify this choice. Moreover, for an indication of the choice of L, the comparative plot depicted in Fig. 13(b) of the squared extensibility L^2 and $R_i = \mathrm{Tr}(\mathbf{A}_i)$, which represents the average length per mode, i.e., of the polymer chain, shows that an

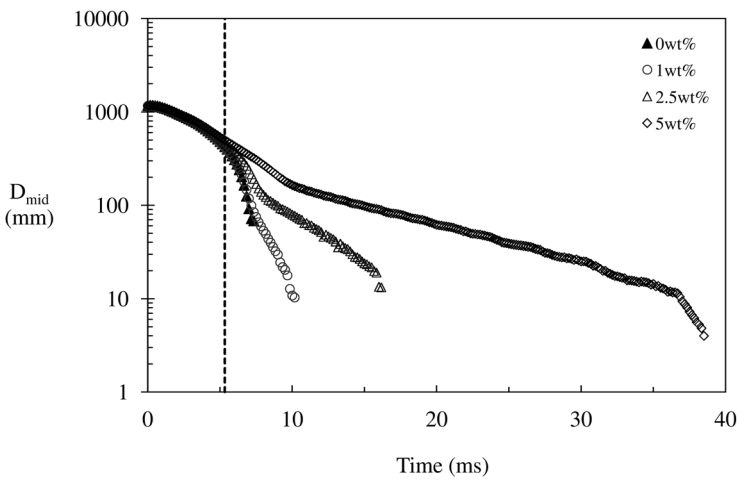

FIG. 6. Time evolution of midfilament taken from photographs of Fig. 2. (▲) DEP, (○) DEP-1 wt. % PS110, (Δ) DEP-2.5 wt. % PS110, (◆) DEP-5 wt. % PS110, and (- - -) piston cessation of motion.

Downloaded 22 Dec 2012 to 109.154.120.51. Redistribution subject to SOR license or copyright; see http://www.journalofrheology.org/masthead

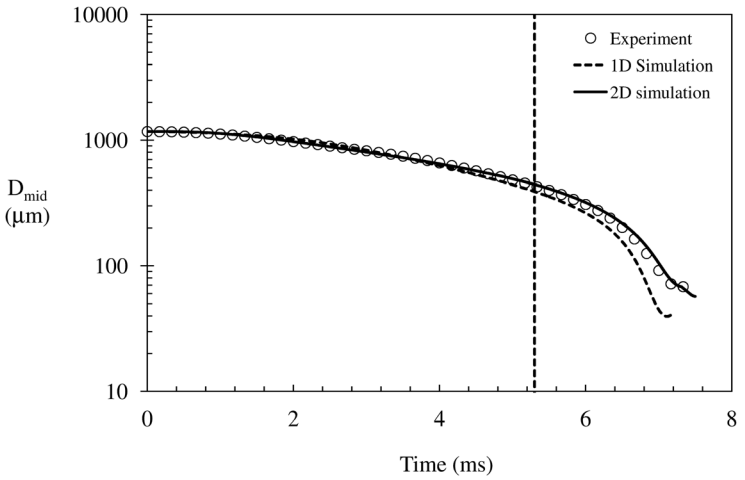

FIG. 7. Newtonian base case. Plot of the midfilament diameter evolution as a function of time. Vertical line corresponds to piston cessation of motion.

extensibility value of around 30 is an appropriate choice. The fifth mode seems to capture the polymer global chain unraveling mechanism, which takes place at larger length scales. On the other hand, the other modes (1–3) with negligible values of R_i involve local changes of the molecular conformation. It is worth noting as well that the R_i axial evolution confirms that higher stretching occurs in the middle of the filament.

The capillary thinning of viscoelastic fluid is controlled by the longest relaxation time with a midfilament diameter decreasing in the form of $D(t) \sim \alpha.\exp(-t/3\lambda)$ [Bazilevsky *et al.* (1990)]. Fitting this exponential decay to the experimental data presented in Fig. 6 yields extensional relaxation times λ_{ext} of 0.425 ms, 1.19 ms, and 3.2 ms for 1, 2.5, and 5 wt. %, respectively. The extensional relaxation λ_{ext} increased with polymer loading as expected. While both the 1D and the 2D simulations match the 1% solution data shown in Fig. 8, there is a progressive mismatch in both decay and pinch off with increasing concentration shown in Figs. 9 and 10. In particular, the decay immediately after piston cessation is overpredicted by both 1D and 2D simulations. Perhaps surprisingly, both the 1D and the 2D simulations give a similar response. It was speculated that the differences may appear between single mode and multimode models because of the existence of shorter and longer modes and of their interactions close to capillary pinch off in the vicinity of both pistons [Matallah *et al.* (2007)].

In the 1D paper [Tembely *et al.* (2012)], single mode modeling was only used; however both a short mode obtained from the PAV data and a long mode obtained from matching with experiment were used. In that paper, it was shown that the smallest relaxation time as input in a nonlinear model was unable to correctly predict filament thinning while the longest relaxation time gave reasonable filament thinning results but a large discrepancy with the experimental G' and G'' data. In this paper, incorporation of multimodes has been carried out in order to fit with greater accuracy the filament thinning experimental results while also capturing the PAV data too. We have chosen five modes in order to have one mode per decade over the range of interest covered experimentally. The exact choice of the number of modes is a matter of details to be emphasized. Two would be too few and eight probably too many.

In this paper, our objective is to predict, using the same nonlinear constitutive equation as in the previous paper, the results for extension solely from experimental data

Downloaded 22 Dec 2012 to 109.154.120.51. Redistribution subject to SOR license or copyright; see http://www.journalofrheology.org/masthead

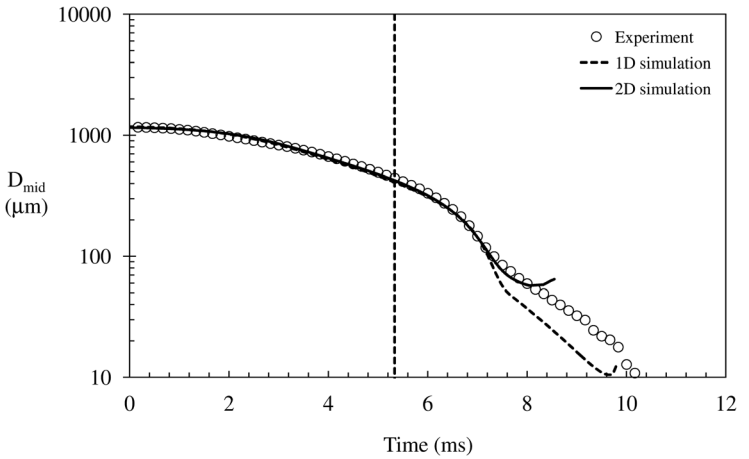

FIG. 8. Single mode, 1 wt. % PS110 in DEP solution. Plot of the midfilament diameter evolution as a function of time. Constitutive equation: Fene-CR, relaxation time $\lambda = 0.425$ ms, shear modulus $g = 11.25$ Pa, and polymer extensibility $L = 30$. Initial gap size: 0.6 mm, final gap size: 1.4 mm, pistons relative velocity: 150 mm/s. Vertical line corresponds to piston cessation of motion (aspect ratio 2.3).

measured in the LVE regime. For that purpose, the oscillatory LVE data were then fitted to a multimode model with five modes spaced by a decade between the modes and the fitted parameters are given in Table II. These multimode parameters were then used in both the 1D and the 2D simulations using the multimode FENE-CR constitutive equations (9) and (10). The results are shown in Figs. 11, 12, and 14 for the 1%, 2.5%, and 5% solutions, respectively. The fit at all concentrations is now greatly improved from the single mode simulations over the whole decay and again there appears to be little difference between the 1D and the 2D simulations.

Using a multimode Maxwell model approach allows better accounting for the transition between visco-capillary thinning and elasto-capillary thinning as shown by the large reduction of the swelling at time between 7 and 10 ms. This constituted the main limitation of the single mode Maxwell approach as shown above and recently reported results by

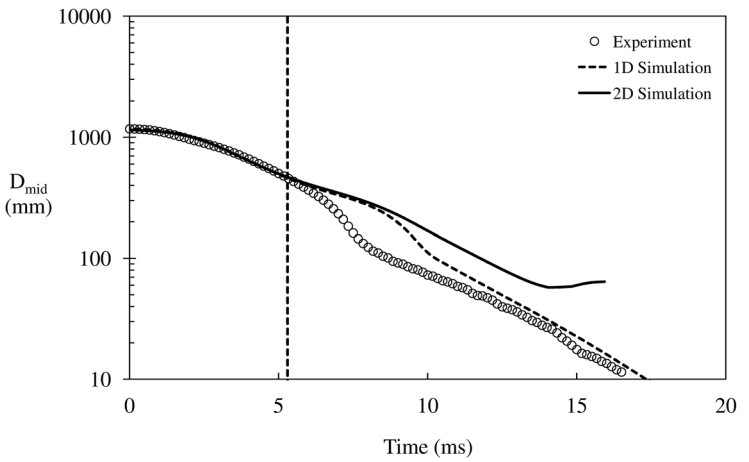

FIG. 9. Single mode, 2.5 wt. % PS110 in DEP solution. Plot of the midfilament diameter evolution as a function of time. Constitutive equation: Fene-CR, relaxation time $\lambda = 1.19$ ms, shear modulus $g = 15$ Pa, and polymer extensibility $L = 30$. Vertical line corresponds to piston cessation of motion.

Downloaded 22 Dec 2012 to 109.154.120.51. Redistribution subject to SOR license or copyright; see http://www.journalofrheology.org/masthead

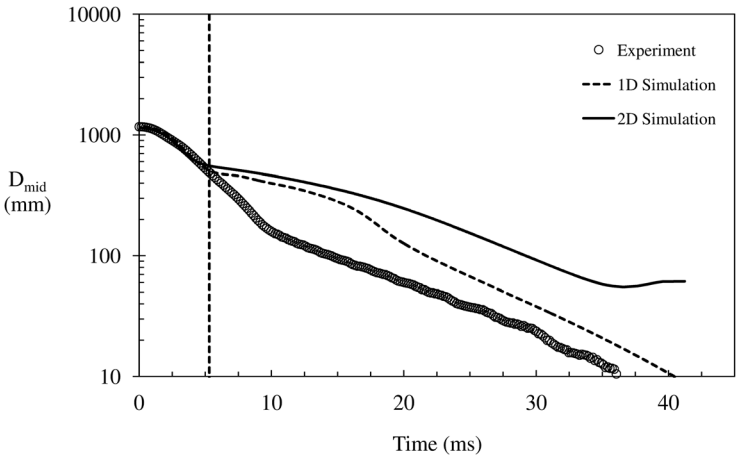

FIG. 10. Single mode, 5 wt. % PS110 in DEP solution. Plot of the midfilament diameter evolution as a function of time. Constitutive equation: Fene-CR, relaxation time $\lambda = 3.2$ ms, shear modulus $g = 17$ Pa, and polymer extensibility $L = 30$. Vertical line corresponds to piston cessation of motion.

some authors of this paper [Tembely *et al*. (2012)]. The results appear to show clearly that a multimode description of the fluid is necessary and that, perhaps surprisingly, the 1D simulation appears to give a closer match to the experimental results. It is also to be emphasized that the multimode approach allows retrieving the results for nonlinear elongation solely with the help of the linear time spectrum and the use of a constitutive equation. It is worth mentioning that mathematically the fitting of the time constant is correct but often leads to poor results, since the relaxation spectrum time is no longer well distributed, and the longest time spectrum may become small. The choice we made by imposing the relaxation time is well accepted and adopted in the literature when dealing with multimode formulation of constitutive equations [see Bird *et al*. (1987)].

The sensitivity of the filament thinning and breakup to constitutive equation and nonlinear parameters is shown in Figs. 14 and 15. In Fig. 14, it can be seen that using the 1D simulation, there is little difference between the multimode FENE-CR and Oldroyd model predictions. Any differences that may appear were essentially masked by the use

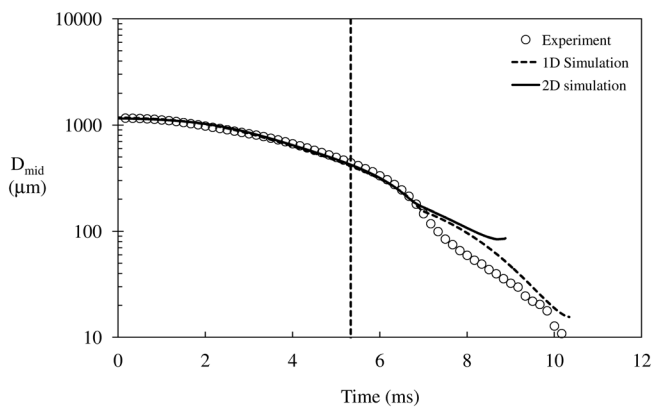

FIG. 11. Multimode, 1 wt. % PS110 in DEP solution. Plot of the midfilament diameter evolution as a function of time. Constitutive equation: Fene-CR, relaxation times λ_i, and shear modulus g_i for the different modes i are given in Table II and polymer extensibility $L = 30$. Vertical line corresponds to piston cessation of motion.

Downloaded 22 Dec 2012 to 109.154.120.51. Redistribution subject to SOR license or copyright; see http://www.journalofrheology.org/masthead

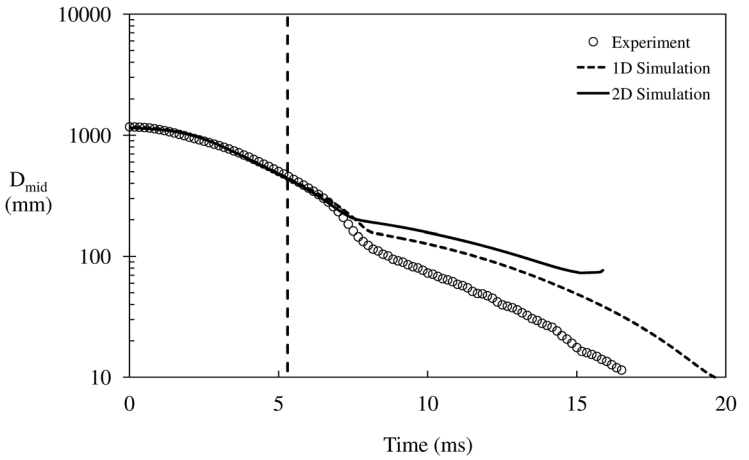

FIG. 12. Multimode, 2.5 wt. % PS110 in DEP solution. Plot of the midfilament diameter evolution as a function of time. Constitutive equation: Fene-CR, relaxation times λ_i, and shear modulus g_i for the different modes i are given in Table II and polymer extensibility $L = 30$. Vertical line corresponds to piston cessation of motion.

of multimodes. Simulation using the theoretically predicted value for the limiting extensibility L of PS110 ($L = 15$), the "best fit" obtained ($L = 30$), and a significantly larger value, here $L = 100$, has been chosen to investigate the effect L of the FENE-CR model. Figure 15 shows that L affect the simulation slightly in the transition zone for the short time modes and particularly in the final stages of decay with a pinch-off time that decreases with decreasing limiting extensibility parameter L.

2. Transient profiles

Figures 16 and 17 present the1D and 2D multimodes FENE-CR and Oldroyd-B full simulated transient profiles for the case of 5 wt. % PS110 diluted in DEP. A generally good match between simulations is observed with differences only appearing toward the end of the filament thinning mechanism, i.e., near to break up. Figure 16 shows that the 1D simulation predicts a final thread like decay, whereas the 2D simulation still has a pinch-off component. The multimode Oldroyd-B simulations shown in Fig. 17 also show a similar trend, with the 1D having a more thread like final decay. Despite the improvement provided by the use of multimodes approach instead of the single mode approach, these results clearly highlight the need for investigating other constitutive equations for the modeling of fast stretching and filament thinning of low viscoelastic fluids.

Detailed full profile comparison between experimental transient profiles of PS110 at 5 wt. % in DEP with FENE-CR multimodes 1D and 2D simulation transient profiles is presented in Fig. 18. Both simulation approaches provide a good match with the experimental profiles for the overall mechanism with again the main discrepancies appearing at the late stage of the filament thinning mechanism. Close examination of the experimental and simulated profiles shows that the fluid regions attached to the top and the bottom pistons are smaller experimentally than for both simulations. This results in a larger length of the thinning filament in the experimental case and may explain the differences observed between 1D and 2D simulations. The filament aspect ratio is usually defined by the variation between initial and final positions of the piston but it can be seen here that despite using similar piston motions for the simulations and the experiments, differences in the filament length arise. Such filament length variations are expected to significantly affect the filament break up profile especially in the case of low viscosity low viscoelastic

Downloaded 22 Dec 2012 to 109.154.120.51. Redistribution subject to SOR license or copyright; see http://www.journalofrheology.org/masthead

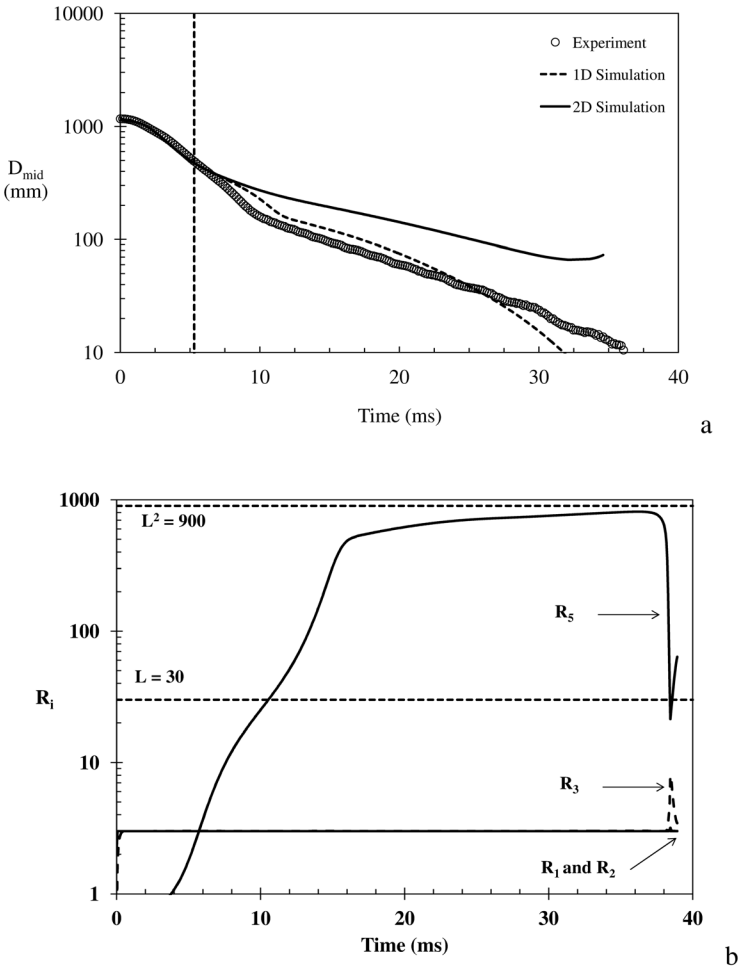

FIG. 13. (a) Multimode, 5% solution. Plot of the midfilament diameter evolution as a function of time. Constitutive equation: Fene-CR, relaxation times λ_i, and shear modulus g_i for the different modes i are given in Table II and polymer extensibility $L = 30$. Vertical line corresponds to piston cessation of motion. (b) Evolution of the R_i as a function of time.

fluids. The investigation of the full velocity field, in terms of simulation and using particle image velocimetry (PIV) experiments, within both the filament and the piston region would help the understanding of the differences observed in the filament shape especially toward the break up time.

3. Weissenberg number W_i and apparent extensional viscosity $\eta_{e,app}$

Figure 19 presents the evolution of the Weissenberg number W_i as a function of the filament thinning Hencky strain ε in the case of multimode FENE-CR simulations. Weissenberg number and filament thinning Hencky strain may be defined as follows:

$$W_i = \lambda_{\text{ext}} \dot{\varepsilon}, \tag{22}$$

$$\varepsilon = 2 \ln\left(\frac{D_0}{D(t)}\right), \tag{23}$$

Downloaded 22 Dec 2012 to 109.154.120.51. Redistribution subject to SOR license or copyright; see http://www.journalofrheology.org/masthead

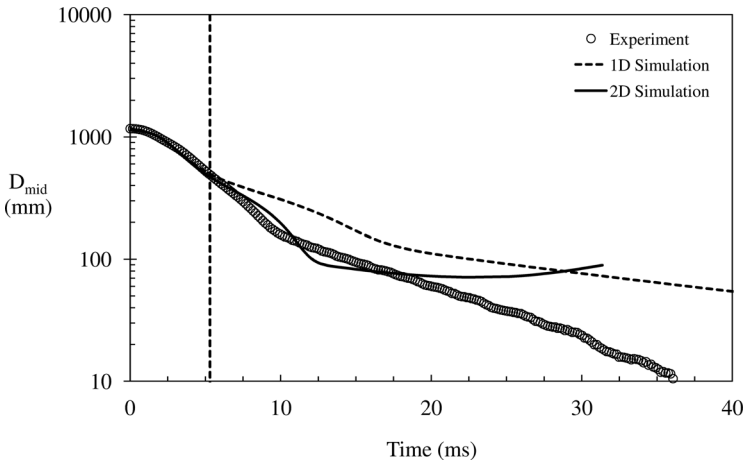

FIG. 14. Multimodes, 5 wt. % PS110 in DEP solution. Plot of the midfilament diameter evolution as a function of time. Constitutive equation: Oldroyd-B, relaxation times λ_i, and shear modulus g_i for the different modes i are given in Table II. Vertical line corresponds to piston cessation of motion.

$$\dot{\varepsilon} = -\frac{2}{D(t)}\frac{dD(t)}{dt}. \tag{24}$$

The simulated data of the midfilament evolution have been used to estimate the longest extensional relaxation time and values of 2.98 ms and 5.1 ms were obtained for the 1D approach and the 2D simulation, respectively, in the case of PS110 at 5 wt. % in DEP.

In the case of the multimode FENE-CR approach, the 1D simulation approach predicts reasonably well the overall mechanism with; in particular, the double curved behavior experimentally observed in the transition between visco-capillary and elasto-capillary regimes ($W_i = 0.5$) whereas the 2D approach provides a good match on the long time scale but does not capture the double curvature. The behavior at high Hencky strain is correctly represented for both types of simulations.

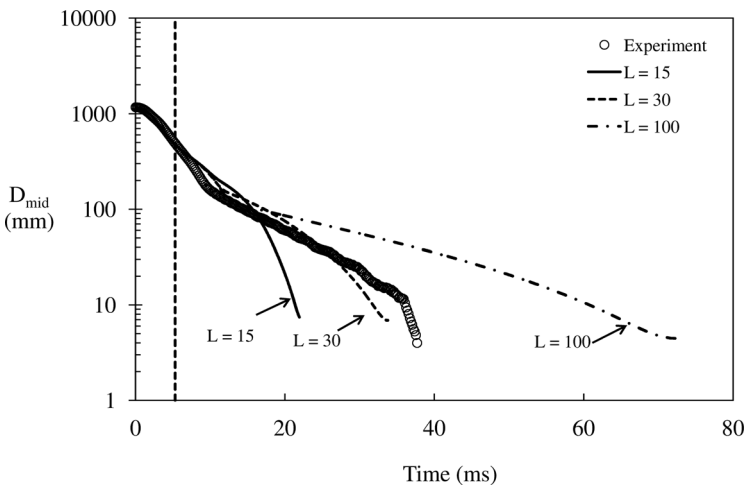

FIG. 15. Effect of extensibility parameter L. Symbols represent the experimental data of the evolution of the midfilament as a function time and lines represent 1D multimode numerical simulations for different polymer chain extensibilities L. Constitutive equation: Fene-CR, relaxation times λ_i, and shear modulus g_i for the different modes i are given in Table II. Vertical line corresponds to piston cessation of motion.

Downloaded 22 Dec 2012 to 109.154.120.51. Redistribution subject to SOR license or copyright; see http://www.journalofrheology.org/masthead

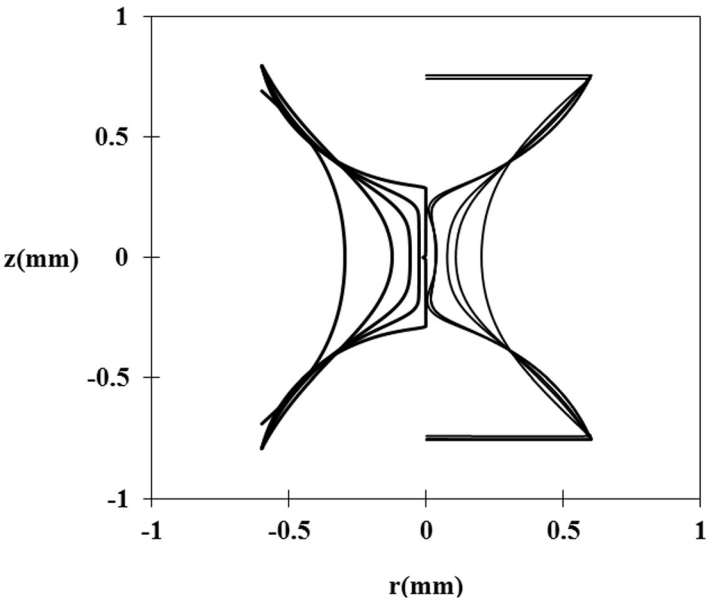

FIG. 16. Comparison between the 1D numerical FENE-CR multimode transient profiles (left), and the corresponding 2D simulations (right) for the DEP + 5% PS. The prescribed times are 5.3 ms, 12 ms, 18.5 ms, 25.5 ms, 38 ms.

The use of the multimode approach does significantly improve the match with experimental data in comparison to that of the single mode and, even if all the subtleties of the complex filament thinning mechanism seem not to be fully represented, it provides good agreement with experimental data. The description of a Weissenberg number, when using

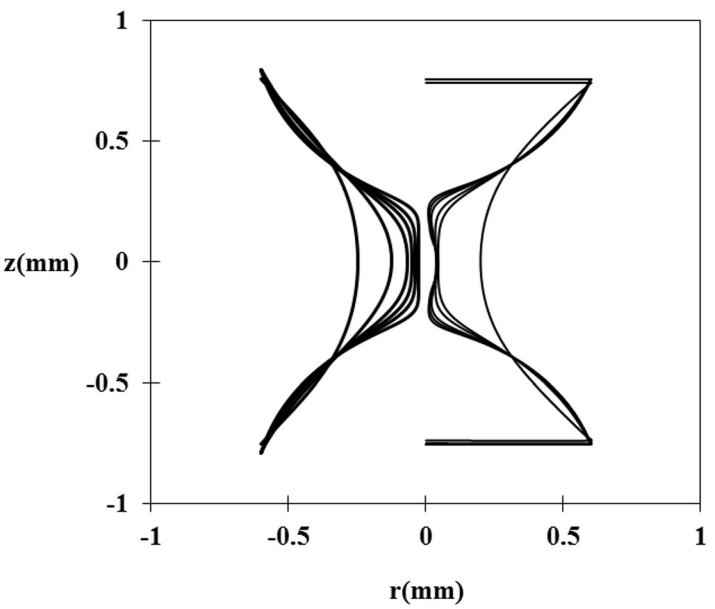

FIG. 17. A comparison between the 1D numerical Oldroyd-B multimode transient profiles (left), and the corresponding 2D simulations (right). The prescribed times are 5.3 ms, 12 ms, 18 ms, 25 ms, 32 ms, and 44 ms for 1D simulation and 5.3 ms, 12 ms, 18 ms, 25 ms, 28 ms, 32.5 ms for 2D simulation.

Downloaded 22 Dec 2012 to 109.154.120.51. Redistribution subject to SOR license or copyright; see http://www.journalofrheology.org/masthead

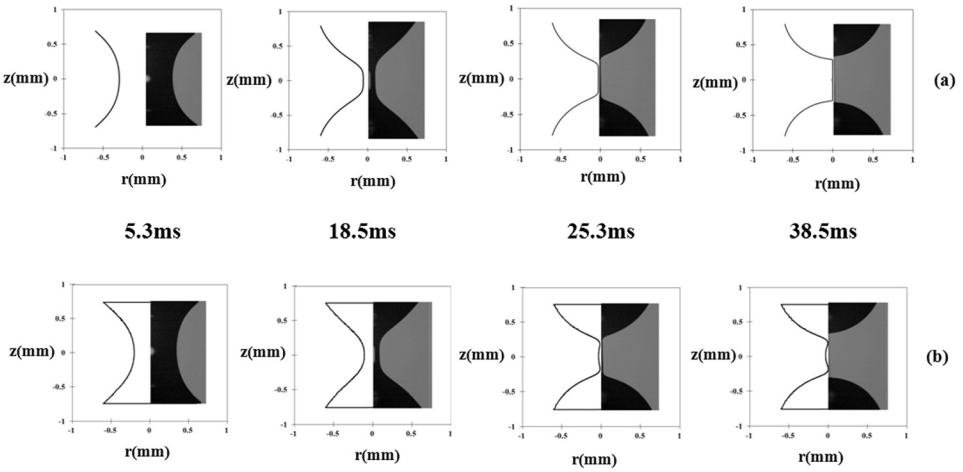

FIG. 18. Comparison between the experimental transient profiles for the DEP + 5 wt. % PS110 and the simulations of (a) the 1D and (b) the 2D cases using the FENE-CR multimode constitutive equations.

a multimode approach, has difficulties in relation to a suitable choice of relaxation time used in the definition of the Weissenberg number. It is also very sensitive to noise (simulation or experimental) due to the fact that it is based on the derivative of the midfilament evolution.

Finally, Fig. 20 presents the transient apparent extensional viscosity $\eta_{e,app}$, with $\eta_{e,app} = -\sigma \frac{dt}{dD_{mid}(t)}$, as a function of Hencky strain for multimode FENE-CR. The comparison is particularly good in view of the approximations which have been made for the calculation of the phenomenological Maxwell times. Notably, the complex behavior of the extensional viscosity is qualitatively correctly predicted at intermediate times by both the 1D and the 2D simulations with the prediction of the sudden increase in η_{ext} after the pistons have stopped. Close attention shows that the 1D simulation approach produces a surprisingly good agreement with experimental results, while the 2D simulation approach fails to represent the long term extensional viscosity behavior.

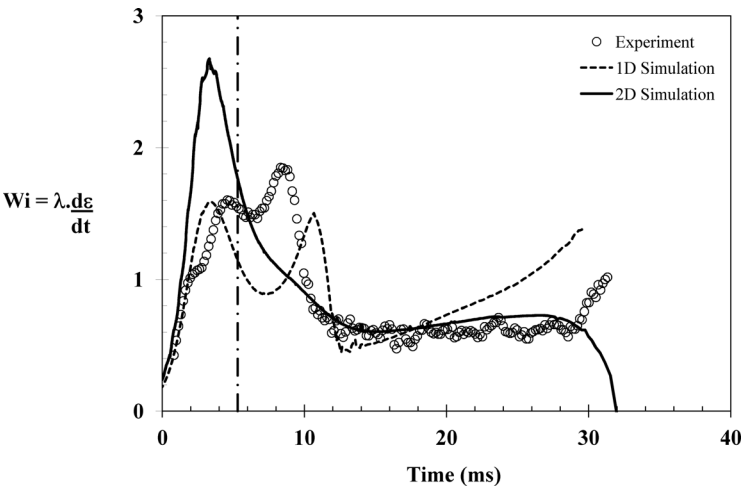

FIG. 19. Evolution of the Weissenberg number as a function of the Hencky strain. Transient Weissenberg numbers were calculated using $\lambda = 3.2$ ms for experimental data, $\lambda = 2.89$ ms and $\lambda = 5.1$ ms for 1D simulation and 2D simulation data using multimodes FENE-CR as constitutive equation.

Downloaded 22 Dec 2012 to 109.154.120.51. Redistribution subject to SOR license or copyright; see http://www.journalofrheology.org/masthead

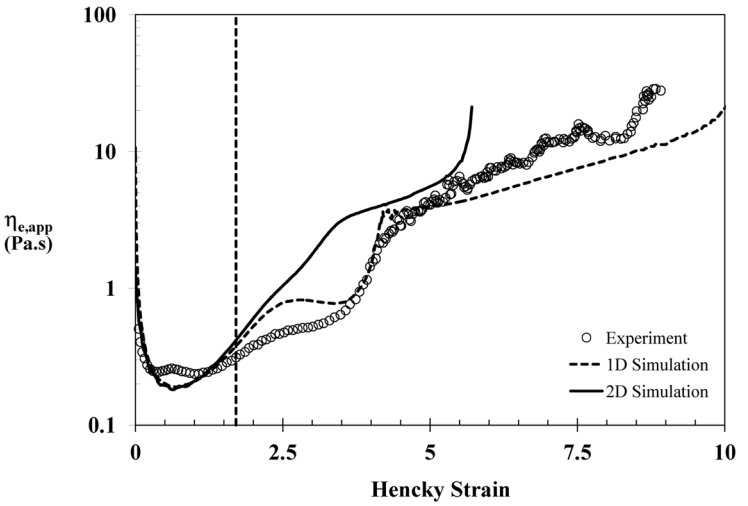

FIG. 20. Evolution of the transient apparent extensional viscosity $\eta_{e,app}$ as a function of the Hencky strain ε for computed from the midfilament evolution shown in Fig. 12.

The relative better accuracy of the 1D model may be due to the combined effect of the ALE technique, for free surface tracking, together with the expression of the full curvature providing means for representing a fully rounded drop. These features together with the low stretching speed, used in this work, enable the 1D model to exhibit quite good results compared to the 2D as previously pointed out by Yildirim and Basaran (2001). Indeed, finding stable discretization schemes for 2D models proves to be most challenging for free surface problems and is computationally more intensive (almost 2 to 3 orders of magnitude compared to 1D models). Finally, the treatment of the tri-junction line (contact between solid/liquid/air) which plays a non-negligible role in the vicinity of pistons is not well-resolved, and this may have a larger effect for the 2D model than that of the 1D model, therefore affecting its overall performance.

V. CONCLUSIONS

Results described in this paper have shown that a multimode constitutive equation approach greatly improves the detailed prediction of viscoelastic extensional flow behavior of dilute or semidilute polymer solutions. The result is consistent with the findings of Entov and Hinch (1997) who also found it necessary to resort to a multimode approach for higher viscosity viscoelastic polymer solutions. However, simulations for different polymer concentrations indicate that the improvement due to the use of multimodes instead of single mode is reduced with the increase of the solution concentration.

The FENE-CR constitutive equation appears to be an effective suitable constitutive equation to use for the fluids examined in this paper, although the Oldroyd model was found to give an equivalent response when used with multimodes. It appears that multimode modeling can disguise certain limiting features of different constitutive models, but however remains necessary even for the monodisperse polymer systems which have been tested. The fitting of numerical simulation to the experimental results was not perfect and this can be attributed to both experimental factors and also weaknesses in the choice of constitutive equations used. This highlight that more physics, or a new set of constitutive equations, needs to be incorporated in the simulations for them to quantitatively match the experimental data.

Downloaded 22 Dec 2012 to 109.154.120.51. Redistribution subject to SOR license or copyright; see http://www.journalofrheology.org/masthead

To be specific on this aspect, more sophisticated models such as the one with elaborate closure relationships for FENE models [Lielens *et al.* (1998)] or the multimode Pom Pom model taking into account molecular topology [McLeish and Larson (1998)] need to be tested. Additional experiments are also needed in order not to have too many adjustable parameters.

An initially surprising result of the paper is the fact that the 1D modeling gives better results than 2D modeling in some limited cases described above. This indicates that the 1D approximation is valid enough for the initial and boundary conditions used and in particular for the midfilament diameter evolution. It is possible (probable?) that when details of highly nonlinear behavior, i.e., pinch-off position, number of beads, etc. are considered differences may emerge from the two techniques. The pinch-off position and the number of small drops are the essential parameters in ink-jet printing since the satellite drops may merge or not following the type of detachment.

Further comparison would be to follow the filament transients following breakup. Such a work has been done for Newtonian liquid [Castrejon-Pita *et al.* (2012)] but this work does not include non-Newtonian fluids. The nonlinear evolution of main drop and satellites do influence printability criterion taking into account the Ohnesorge and the Deborah numbers as described in preliminary work by Tembely *et al.* (2011).

ACKNOWLEDGMENTS

D.V., M.R.M., O.G.H., and N.F.M. would like to acknowledge the financial support of the EPSRC and Industrial Ink Jet Consortium funding. The authors would also like to acknowledge with thanks rheological assistance from Dr. Kathryn Yearsley. M.T. and A.S. wish to acknowledge financial support from ANR PAN'H 2008 CATIMINHY project.

References

Anna, S. L., and G. H. McKinley, "Elasto-capillary thinning and breakup of model elastic liquids," J. Rheol. **45**, 115–138 (2001).

Bach, A., H. K. Rasmussen, P.-Y. Longin, and O. Hassager, "Growth of non-axisymmetric disturbances of the free surface in the filament stretching rheometer: Experiments and simulation," J. Non-Newtonian Fluid Mech. **180**, 163–186 (2002).

Baumgaertel, M., and H. H. Winter, "Determination of discrete relaxation and retardation time spectra," Rheol. Acta **28**(51), 1–519 (1989).

Bazilevsky, A. V., V. M. Entov, and A. N. Rozhkov, "Liquid filament microrheometer and some of its applications," in *Third European Rheology Conference*, edited by D. R. Oliver (Elsevier Applied Science, London and New York, 1990), pp. 41–43.

Bazilevsky, A. V., V. M. Entov, M. M. Lerner and A. N. Rozhkov, "Failure of polymer solutions filaments," Polym. Sci., Ser. A **39**(3), 316–324 (1997).

Bird R. B., R. C. Armstrong, and L. Hassager, *Dynamic of Polymeric Liquids: Fluid Mechanics*, 2nd ed. (John Wiley & Sons, New York, 1987).

Brezzi F., and J. PitkÄaranta, "On the stabilization of finite element approximations of the Stokes equations," in *Efficient Solutions of Elliptic Systems*, edited by W. Hackbush, Vol. 10 of Notes on Numerical Fluid Mechanics (Braunschweig, 1984).

Castrejon-Pita, A. A., J. R. Castrejon-Pita, and I. M. Hutchings, "Breakup of liquid filaments," Phys. Rev. Lett. **108**, 074506 (2012).

Castrejon-Pita, J. R., N. F. Morrison, O. G. Harlen, G. D. Martin, and I. M. Hutchings, "Experiments and Lagrangian simulations on the formation of droplets in continuous mode," Phys. Rev. E **83**, 016301 (2011).

Downloaded 22 Dec 2012 to 109.154.120.51. Redistribution subject to SOR license or copyright; see http://www.journalofrheology.org/masthead

Chilcott, M. D., and J. M. Rallison, "Creeping flow of dilute polymer solutions past cylinders and spheres," J. Non-Newtonian Fluid Mech. **29**, 381–432 (1988).

Clasen, C., J. Eggers, M. A. Fontelos, J. Li, and G. H. McKinley, "The beads-on-string structure of viscoelastic threads," J. Fluid Mech. **556**, 283–308 (2006b).

Clasen, C., J. P. Plog, W.-M. Kulicke, M. Owens, C. Macosko, L. E. Scriven, M. Verani, and G. H. Mckinley, "How dilute are dilute solutions in extensional flows?," J. Rheol. **50**(6), 849–881 (2006a).

Courant, R., K. Friedrichs, and H. Lewy, "Über die partiellenDifferenzengleichungen der mathematischenPhysik," Math. Ann. **100**, 32–74 (1928).

Crassous, J., R. Régisser, M. Ballauff, and N. Willenbacher, "Characterisation of the viscoelastic behaviour of complex fluids using the piezoelastic axial vibrator," J. Rheol. **49**, 851–863 (2005).

Davies A. R., and R. S. Anderssen, "Sampling localization in determining the relaxation spectrum," J. Non-Newtonian Fluid Mech. **73**, 163–179 (1997).

Dong, H., W. W. Carr, and J. F. Morris, "An experimental study of drop-on-demand drop formation," Phys. Fluids **18**, 072102-1–072102-16/ (2006).

Edelsbrunner, H., "Triangulations and meshes in computational geometry," Acta Numerica **9**, 133–213 (2000).

Eggers, J., and T. F. Dupont, "Drop formation in a one-dimensional approximation of the Navier-Stokes equation," J. Fluid Mech. **262**, 205–221 (1994).

Eggers, J., and E. Villermaux, "Physics of liquid jets," Rep. Prog. Phys. **71**, 036601 (2008).

Entov, V. M., and E. J. Hinch, "Effect of a spectrum relaxation times on the capillary thinning of a filament elastic liquids," J. Non-Newtonian Fluid Mech. **72**, 31–53 (1997).

Ferry, J. D., *Viscoelastic Properties of Polymers* (John Wiley & Sons, Inc., New York, 1980).

Furlani, E. P., and M. S. Hanchak, "Nonlinear analysis of the deformation and breakup of viscous microjets using the method of lines," Int. J. Numer. Methods Fluids **65**(5), 563–577 (2011).

Groß, T., L. Kirschenmann, and W. Pechhold, "Piezo axial vibrator (PAV)—A new oscillating squeeze flow rheometer," in *Proceedings Eurheo*, edited by H. Munsted, J. Kaschta, and A. Merten (European Society of Rheology, Erlangen, 2002).

Harlen, O. G., J. M. Rallison, and P. Szabo, "A split Langrangian-Eulerian method for simulating transient viscoelastic flows," J. Non-Newtonian Fluid Mech. **60**, 81–104 (1995).

Hoath, S. D., G. D. Martin, T. R. Tuladhar, M. R. Mackley, I. Hutching, and D. Vadillo, "Link between ink rheology, drop-on-demand jet formation and printability," J. Imaging Sci. Technol. **53**(4), 041208-1–041208-8 (2009).

Jang, D., D. Kim, and J. Moon, "Influence of fluid physical properties on ink-jet printability," Langmuir **25**, 2629–2635 (2009).

Jorge N., and S. J. Wright, *Numerical Optimization*, 2nd ed. (Springer, 2006).

Kamath, V., and M. R. Mackley, "The rheometric characterization of flexible chain and liquid crystal polymers," in *3rd European Rheology Conference*, edited by D. R. Oliver (British Society of Rheology, London and New York, 1990), pp. 261–264.

Kirschenmann, L., Ph.D. thesis, Institut fur Dynamischematerialprunfung (IdM), University of Ulm, 2003.

Lielens, G., P. Halin, I. Jaumain, R. Keunings, and V. Legat, "New closure approximations for the kinetic theory of finitely extensible dumbbells," J. Non-Newtonian Fluid Mech. **76**, 249–279 (1998).

Matallah, H., K. S. Sujatha, M. J. Banaai, and M. F. Webster, "Single and multi-mode modelling for filament stretching flows," J. Non-Newtonian Fluid Mech. **146**, 92–113 (2007).

McKinley, G. H, "Dimensionless groups for understanding free surface flows of complex fluids," Soc. Rheol. Bull. **74**(2), 6–10 (2005a).

McKinley, G. H., "Visco-elastic-capillary thinning and break-up of complex fluid," in *Rheology Reviews 2005*, (The British Society of Rheology, 2005b), pp. 1–48.

McKinley, G. H., and T. Sridhar, "Filament stretching rheometry of complex fluids," Annu. Rev. Fluid Mech. **34**, 375–415 (2002).

McLeish, T. C. B., and R. G. Larson, "Molecular constitutive equations for a class of branched polymers: The pom-pom polymer," J. Rheol. **42**, 81–110 (1998).

Morrison, N. F., and O. G. Harlen, "Viscoelasticity in inkjet printing," Rheol. Acta **49**, 619–632 (2010).

Paige, C. C., and M. A. Saunders, "Solution of sparse indefinite systems of linear equations," SIAM J. Numer. Anal. **12**(4), 617–629 (1975).

Downloaded 22 Dec 2012 to 109.154.120.51. Redistribution subject to SOR license or copyright; see http://www.journalofrheology.org/masthead

Schittkowski, K., "NLQPL: A FORTRAN-subroutine solving constrained nonlinear programming problems," Annals of Operations Research **5**, 485–500 (1985).

Shi, X. D., M. P. Brenner, and S. R. Nagel, "A cascade of structure in a drop falling from a faucet," Science **265**, 219 (1994).

Stadler, F. J., and C. Bailly, "A new method for the calculation of continuous relaxation spectra from dynamic-mechanical data," Rheol. Acta **48**(1), 33–49 (2009).

Tembely, M., D. Vadillo, M. R. Mackley, and A. Soucemarianadin, "Towards an optimization of DOD printing of complex fluids," Non Impact Printing Conference, Salt Lake City, UT (IS&T, Springfield, 2011).

Tembely, M., D. C. Vadillo, M. R. Mackley, and A. Soucemarianadin, "The matching of a "one-dimensional" numerical simulation and experiment results for low viscosity Newtonian and non-Newtonian fluids during fast filament stretching and subsequent break-up," J. Rheol. **56**, 159–184 (2012).

Vadillo, D. C., T. R. Tuladhar, A. Mulji, and M. R. Mackley, "The rheological characterisation of linear viscoelasticity for ink jet fluids using a piezo axial vibrator (PAV) and torsion resonator (TR) rheometers," J. Rheol. **54**(4), 781–799 (2010a).

Vadillo, D. C., T. R. Tuladhar, A. C. Mulji, S. Jung, S. D. Hoath, and M. R. Mackley, "Evaluation of the inkjet fluid's performance using the 'Cambridge Trimaster' filament stretch and break-up device," J. Rheol. **54**(2), 261–282 (2010b).

Vadillo, D. C., W. Mathues, and C. Clasen, "Microsecond relaxation processes in shear and extensional flows of weakly elastic polymer solutions," Rheol. Acta **51**, 755–769 (2012).

Wathen, A., and D. Silvester, "Fast iterative solution of stabilized stokes systems using simple diagonal preconditioners," SIAM J. Numer. Anal. **30**, 630–649 (1993).

Westborg, H., and O. Hassager, "Creeping motion of long bubbles and drops in capillary tubes," J. Colloid and Interfacial Sci. **33**(6), 135–147 (1989).

Yao, M., and G. H. McKinley, "Numerical simulation of extensional deformations of viscoelastic liquid bridges in filament stretching devices," J. Non-Newtonian Fluid Mech. **74**, 47–88 (1998).

Yildirim, O. E., and O. A. Basaran, "Deformation and breakup of stretching bridges of Newtonian and shear-thinning liquids: Comparison of one- and two-dimensional models," Chem. Eng. Sci. **56**(1), 211–233 (2001).

Downloaded 22 Dec 2012 to 109.154.120.51. Redistribution subject to SOR license or copyright; see http://www.journalofrheology.org/masthead